PRAMANA — journal of physics

© Indian Academy of Sciences

Vol. 84, No. 6
June 2015
pp. 957–966

Understanding metal–insulator transition in sodium tungsten bronze

SANHITA PAUL and SATYABRATA RAJ*

Department of Physical Sciences, Indian Institute of Science Education and Research-Kolkata, Mohanpur Campus, Nadia 741 246, India

*Corresponding author. E-mail: raj@iiserkol.ac.in

DOI: 10.1007/s12043-015-0993-9; ***e*Publication:** 20 May 2015

Abstract. We have carried out angle-resolved photoemission spectroscopy (ARPES) and spectromicroscopy studies to understand the metal–insulator transition (MIT) observed in sodium tungsten bronzes, Na_xWO_3. The experimentally determined band structure is compared with the theoretical calculation based on full-potential linear augmented plane-wave method. It has been found that there is a good gross agreement between experiment and theory. ARPES spectra on the insulating sample show that the states near E_F are localized due to the random distribution of Na in WO_3 lattice which causes strong disorder in the system. Our spectromicroscopy measurements on both insulating and metallic samples do not approve percolation model to explain MIT in Na_xWO_3. Photoemission spectroscopy on metallic samples does not show any Na-induced impurity band (level), which was one of the models to explain MIT. Electron-like Fermi surface(s) has been found from our experiment for metallic samples at the Γ(X) point which shows good agreement with band calculation.

Keywords. Photoemission spectroscopy; metal–insulator transition; band structure; Fermi surface.

PACS Nos 79.60.−i; 71.30.+h; 71.18.+y

1. Introduction

Materials with potential for technological applications always create huge interest among material scientists. Alkali-doped tungsten oxide (WO_3) is one such material which has a wide range of technological applications. Therefore, its electronic structure and transport properties have been studied by many scientists around the world [1,2]. Although all types of alkali-doped WO_3 have been reported in literature, only sodium (Na) doped WO_3 (i.e. Na_xWO_3, where $0 < x < 1$) has been studied extensively compared to others over the last few decades not only for its technological applications but also from the fundamental prospective. Initial interest on Na_xWO_3 among material scientists was due to its very interesting optical properties, i.e. the colour of Na_xWO_3 changes from greenish

yellow to golden yellow with changing Na concentration in bulk WO_3 matrix as shown in figure 1a [3]. Along with interesting optical properties, Na_xWO_3 also has rich phase diagram and the crystal structure changes from monoclinic to cubic as a function of Na concentration at room temperature [4]. For high Na doping ($x > 0.25$) in WO_3, Na_xWO_3 forms a distorted perovskite structure, where the Na ions occupy the centre of the cube and the WO_6 octahedra occupy the cube corners as shown in figure 1b. Apart from the interesting optical properties and rich phase diagram, the most significant fundamental electronic property exhibited by Na_xWO_3 is the metal–insulator transition (MIT) with Na doping (x). The MIT, one of the interesting and highly studied topics in condensed matter physics, is observed in many strongly correlated transition metal compounds. Various effects, such as electron–electron interaction, disorder due to doping and formation of impurity bands/states are mainly responsible for MIT leading to localization and delocalization of conduction electrons. When Na is doped to WO_3, the 3*s* electron of Na goes to 5*d* of W and the system should be metallic for any small amount of Na doping but it has been found from the transport measurements that Na_xWO_3 becomes insulating for low Na doping ($x < 0.25$), whereas it shows metallic characteristics for high doping values [5]. For a long time, the origin of this insulating phase was not clear and several models were proposed to explain the cause responsible for this MIT in Na_xWO_3. Different possible models for MIT are described schematically in figure 2. In the context of MIT in Na_xWO_3, the idea of percolation-driven mechanism was thought for a long time [6]. Na is doped randomly over the WO_3 lattice and the metallic conduction occurs above the percolation threshold. So, as per the percolation model, large metallic domains of Na_xWO_3 with very high x are embedded in the insulating WO_3 for the above critical Na concentration. As Na donates its 3*s* electron to W 5*d* orbitals, strong correlation effect of 5*d* conduction electrons can also be a reason behind MIT leading to the formation of lower Hubbard band (LHB) and upper Hubbard band (UHB). In Na_xWO_3, Anderson localization model [7] explains MIT because of the strong disorder arising from random distribution of the dopant Na^+ ions in the WO_3 bulk lattice. This strong disorder makes all the states near the conduction band tail localized with a mobility edge (E_c). If the Fermi level (E_F) lies below the mobility edge, then the system becomes insulating and the system becomes metallic as E_F crosses the E_c for higher doping. Na in WO_3 can induce the impurity band [8] where the states become localized for low Na concentration and can explain MIT similar to doped semiconductors. The MIT is associated with the localization

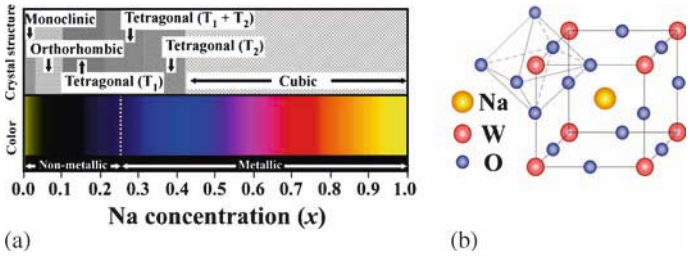

Figure 1. **(a)** Schematic view of crystal structures and optical properties of Na_xWO_3 with Na concentration (x). **(b)** Cubic crystal structure of $NaWO_3$ showing corner sharing WO_6 octahedra.

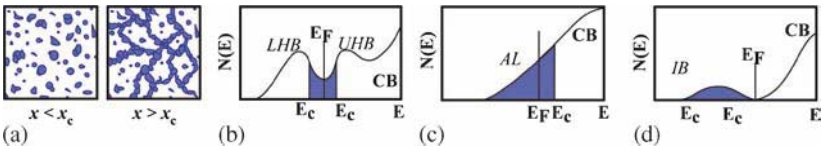

Figure 2. Schematic diagram of different models for MIT in Na_xWO_3. **(a)** Percolation-driven metal–insulator transition where the Na-doped metallic domains grow in size and joins each other for $x > x_c$ (x_c = critical concentration) to give a smooth connectivity leading to MIT. **(b)** Strong electron correlation effect leading to LHB and UHB. **(c)** Anderson localization at conduction band tail. **(d)** Formation of Na-induced impurity band.

and delocalization of states in a very narrow energy range close to E_F in Na_xWO_3. Therefore, high-resolution photoemission spectroscopic and spectromicroscopic studies of metallic and insulating Na_xWO_3 are required to achieve a better understanding of the electronic structure of this type of system. These investigations also help us to understand the mechanism behind the MIT in Na_xWO_3.

2. Crystal growth and experimental techniques

2.1 *Single crystal growth and characterization*

Insulating Na_xWO_3 ($x = 0.025$) single crystals were grown from the high temperature solution 15 mol% Na_2O with WO_3 by a slow cooling method [9], whereas fused salt electrolysis of Na_2WO_4 and WO_3 was used to synthesize metallic single crystals of Na_xWO_3 ($x = 0.7$ and 0.8) as described by Shanks [10]. Transport measurements, Laue diffraction and scanning electron microscopy (SEM) have confirmed that the samples are metallic with a single phase.

2.2 *Spectromicroscopy*

Spectromicroscopy is the microscopy with a definite kinetic energy of photoelectron spectra where a very narrow incident photon beam with submicron spatial resolution is used. Spectromicroscopic experiments were performed on the spectromicroscopy beamline at the Elettra Synchrotron light source with an incident photon energy of 27 eV [11]. To focus the photon beam on the sample, a Schwarzschild objective which brings down the beam spot size to 0.5 μm was used [12]. A schematic view of the spectromicroscopic experimental set-up is shown in figure 3a. Measurements were performed at room temperature in a vacuum better than 2×10^{-10} mbar.

2.3 *Angle-resolved photoemission spectroscopy (ARPES)*

ARPES is the most direct method to study the electronic band structure of solids. The basic principle of ARPES can be explained by Einstein's photoelectric effect [13], which is basically a photon-in and electron-out process. When highly energetic photons shine

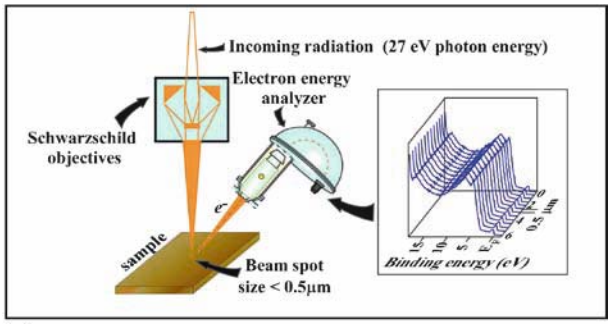

(a)

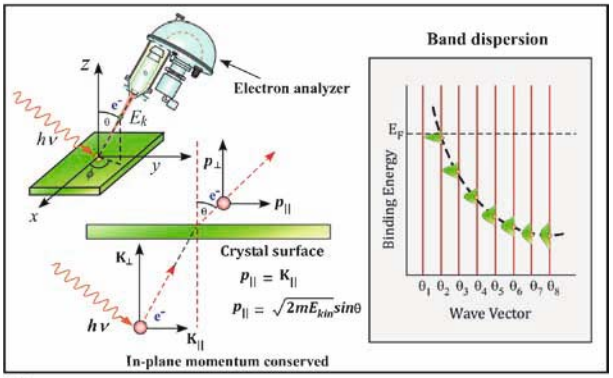

(b)

Figure 3. **(a)** Schematic view of the experimental set-up of the spectromicroscopic measurements. A Schwarzschild objective is used to focus the photon beam on the sample, down to a submicron size spot with a spatial resolution of less than 0.5 μm. **(b)** Schematic diagram showing the principle of angle-resolved photoemission spectroscopy (ARPES). The kinetic energy and angle of emitted photoelectrons with respect to the surface normal are measured by ARPES and therefore, the band dispersions in the material are directly mapped by this method.

on the sample surface, the inside electrons absorb the energy of the photon and come out with a particular kinetic energy and momentum (see figure 3b). ARPES measures the kinetic energy and angle of emitted photoelectrons with respect to the surface normal. The parallel component of the outcoming photoelectron is generally conserved whereas due to the broken translational symmetry along the vertical direction, $k_\perp$ is not conserved. Due to conservation laws of energy and momentum in photoemission process, one can measure simultaneously both the energy and momentum of electrons in solids which gives the band dispersion. ARPES measurements were performed in photoemission laboratory of Tohoku University, Japan [14–16] and also in BadElPh beamline and APE beamline of Elettra Synchrotron, Trieste, Italy [17,18]. Laboratory-based He I photons ($h\nu = 21.218$ eV) and synchrotron radiations were used to excite photoelectrons. The energy and angular (momentum) resolutions were set at 5–25 meV and 0.2° respectively. The measurements were performed at 10–300 K in a vacuum better than 5×10^{-11}

Torr base pressure. The Fermi level of the sample was compared to that of a gold film evaporated on the sample substrate.

3. Results and discussions

Percolation theory is one of the proposed models to elucidate the mechanism behind MIT in Na_xWO_3, and to verify this model, we have carried out spectromicroscopic measurements of both insulating ($x = 0.025$) and metallic ($x = 0.7, 0.8$) compositions [11]. It is essential to study the spectromicroscopic image close to Fermi edge as all the states close to E_F are responsible for MIT. Images collected over $100 \times 100\ \mu m^2$ areas of the sample surface of insulating ($x = 0.025$) and metallic ($x = 0.8$) Na_xWO_3 are shown in figures 4a and 4b, respectively. We find a visible colour contrast (yellow colour denotes the highest intensity while black denotes the lowest intensity) in the image. To understand whether they are from the variation of the spectral feature or not, we have taken the near-E_F spectra at different spots as marked in figures 4c and 4d for insulating and metallic Na_xWO_3, respectively. All the spots of the images are checked carefully and each photoemission spectrum is compared to find out the existence of any embedded metallic domains with finite DOS at E_F in insulating Na_xWO_3 or any embedded insulating domains within metallic structure in metallic Na_xWO_3. In the insulating sample all the spectra are equivalent and the DOS near E_F gradually decreases and vanishes at E_F. Metallic domains do not exist in the insulating host of Na_xWO_3 ($x = 0.025$) within

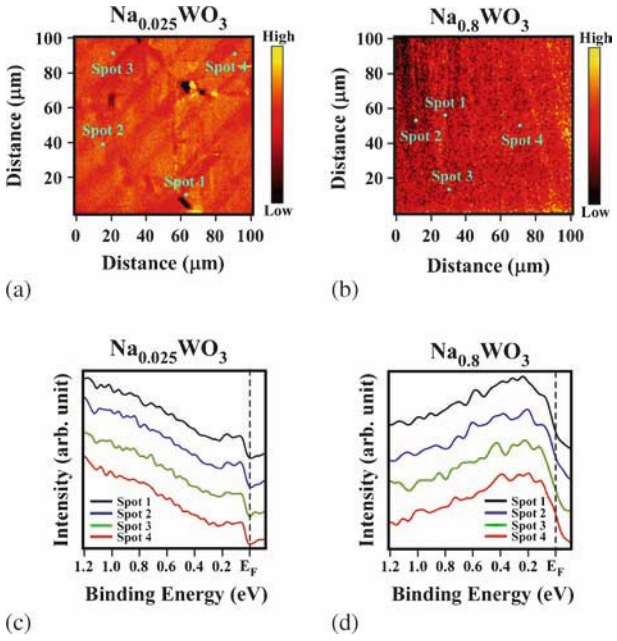

Figure 4. Spectromicroscopic images collected over $100 \times 100\ \mu m^2$ area in **(a)** insulating $Na_{0.025}WO_3$ and **(b)** metallic $Na_{0.8}WO_3$ sample surfaces close to E_F. Photoemission spectra of **(c)** insulating $Na_{0.025}WO_3$ and **(d)** metallic $Na_{0.8}WO_3$ close to E_F taken at different selected spots marked in their corresponding images.

the experimental limit of spatial resolution. As in the insulating sample, the Na doping is quite small, to validate the percolation theory one expects to see the signature of non-metallic spectra in metallic sample, where Na doping is quite high, i.e. $x = 0.8$. It has been found that all the spectra have finite DOS at E_F showing the metallic character of the sample. Hence, insulating domain does not exist in the metallic host of Na_xWO_3 ($x = 0.8$) within the experimental spatial limit of less than one micron. The colour contrast appearing in the images is topographical and arises from a bad focus of the electron analyser with an uneven/step-like sample surface (generated due to sample cleaving). So we conclude from our spectromicroscopic study that percolation model is not a suitable model to explain MIT in Na_xWO_3. Another possibility to explain the MIT is the splitting of the band due to electron correlation at the chemical potential (E_F) into LHB and UHB. Such scenario is unlikely in the case of Na_xWO_3 as originally proposed by Mott [19]. Such splitting of band is highly applicable if the band has integral occupancy, whereas insulating property in Na_xWO_3 is observed for all composition of Na doping below 0.25. Moreover, the correlation effect (U) is expected to be weak and tungsten 5d bandwidth (W) is quite large to satisfy Mott–Hubbard criterion of $U/W \gg 1$.

Figure 5 shows the band structure of insulating Na_xWO_3 for $x = 0.025$ measured by ARPES at 130 K. The valence band structure as shown in figure 5a has been obtained by taking the second derivative of the ARPES spectra. As mentioned earlier, E_F lies in the conduction band for all compositions of Na_xWO_3. It has been found that the bottom of the conduction band lies at 0.5 eV binding energy, whereas the top of the valence band extends

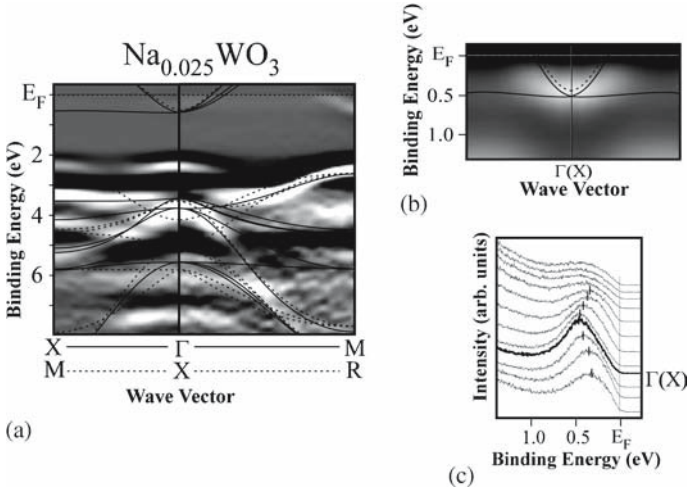

Figure 5. **(a)** ARPES-derived experimental valence-band structure of $Na_{0.025}WO_3$ along the high symmetry X-Γ-M and M-X-R directions in the first Brillouin zone measured at 130 K. Bright areas correspond to the experimental bands. The FP-LAPW band calculation is also shown by solid and dashed lines for comparison with experimental band structure. **(b)** Near-E_F ARPES spectral intensity plot of $Na_{0.025}WO_3$ around Γ(X) point along Γ(X)-X(M) symmetry direction as a function of binding energy and wave vector. An electron pocket is found around the Γ(X) point. **(c)** ARPES spectra near E_F showing dispersion of the peak around the Γ(X) point. Vertical bars are guides to the eyes for band dispersion.

up to 2.5 eV. The energy gap of ∼2 eV between the valence and the conduction bands corresponds to the hard band gap observed in insulating WO_3. To understand this more clearly, it is very important to address the similarity and differences in band structures of WO_3 and $NaWO_3$. Therefore, we carried out theoretical band calculations for WO_3 and $NaWO_3$ by first principle all-electron full potential linear augmented plane-wave (FP-LAPW) method [20,21] within the framework of density functional theory. WO_3 can be assumed to have a pseudocubic crystal structure compared to its real monoclinic structure. Therefore, we have considered cubic crystal structure with lattice parameter $a = 3.78$ Å and 3.85 Å for WO_3 and $NaWO_3$, respectively for our calculations. We have performed our calculations within the local spin density approximation (LSDA) for the exchange using a k-points mesh of $20\times20\times20$. Figures 6a and 6b show the band structures of WO_3 and $NaWO_3$, respectively along the high symmetry X-Γ-M and Γ-X-R directions of the Brillouin zone. From calculations, it has been found that WO_3 is a band insulator and E_F lies inside the band gap (see figure 6a). Na donates its 3*s* electron to the W 5*d* t_{2g} orbitals when Na is doped into WO_3 lattice in $NaWO_3$ and the system becomes metallic as shown in figure 6b. The conduction band of both WO_3 and $NaWO_3$ has a contribution from the W 5*d* t_{2g} states whereas the valence band comprises O 2*p* states. We have superimposed FP-LAPW band calculation of cubic WO_3 on experimental band mapping for comparison. It has been found that there is a good agreement between the theoretical and experimental band structures. However, top of the valence band at 2.5 eV around Γ(X) point is not predicted in the band calculation. To understand in detail the mechanism of MIT, one has to focus on the band structure near E_F region. Hence, we plot the ARPES intensity near E_F around Γ point as shown in figure 5b. An electron-like pocket around the Γ(X) point has been found, whose dispersion agrees satisfactorily with the band calculation. It should be noted here that the conduction band arises from W 5*d* t_{2g} orbitals as explained from our theoretical calculations. The peak at ∼0.5 eV around Γ(X) disperses upward which is clearly visible in figure 5c but never crosses E_F showing the insulating behaviour. A similar feature was also observed at both X(M) and M(R) points (not shown) and was explained by surface reconstruction [15]. The observed

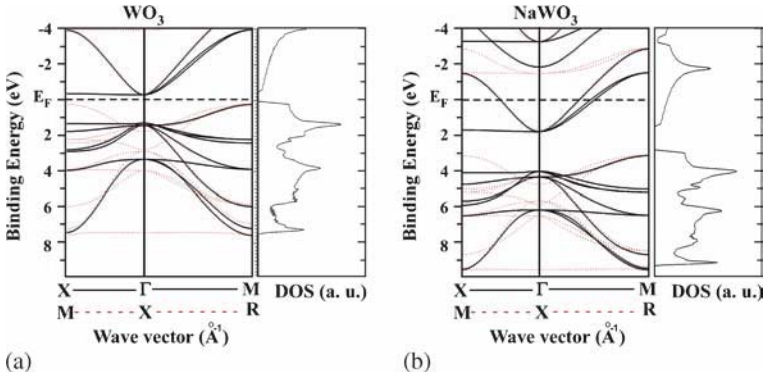

Figure 6. Electronic band structures and density of states (DOS) of **(a)** WO_3 and **(b)** $NaWO_3$ calculated by FP-LAPW method along the high symmetry X-Γ-M (solid line) and M-X-R (dotted line) directions of the first Brillouin zone.

insulating behaviour is the result of Anderson localization of all states in the conduction band due to the strong disorder arising from random distribution of Na in Na_xWO_3. A pure Anderson localization should not open any gap but due to the long-range interaction of the conduction electrons, a soft Coulomb gap arises at E_F and as a result DOS

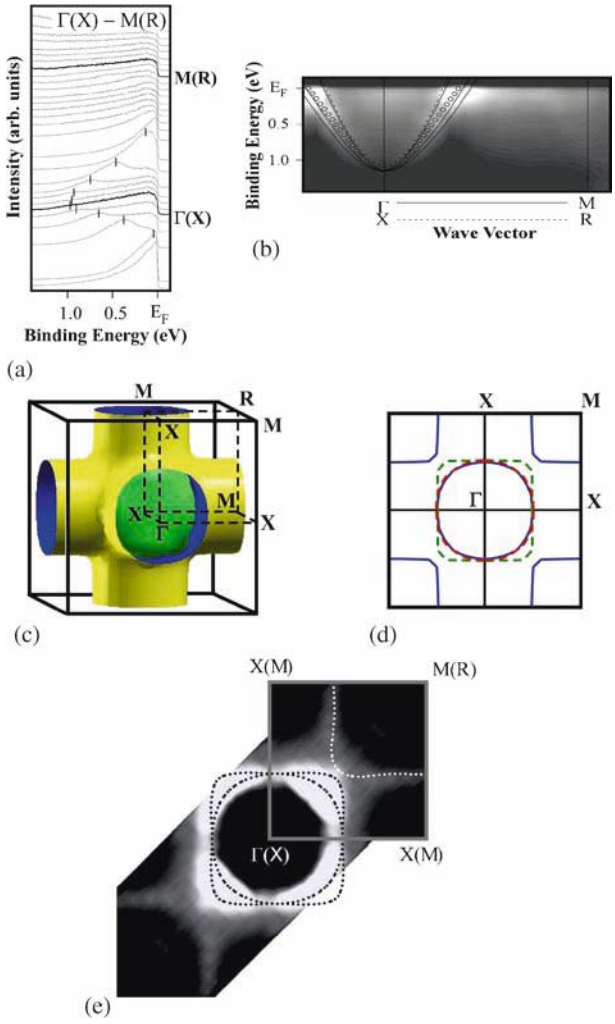

Figure 7. **(a)** Experimental near-E_F spectra of $Na_{0.8}WO_3$ measured at 14 K along the Γ(X)-M(R) direction of the Brillouin zone. Vertical bars are guides to the eyes for band dispersion. **(b)** Near-E_F ARPES spectral intensity plot of $Na_{0.8}WO_3$. An electron-like band is clearly visible around the Γ(X) point. Theoretical band structure of $NaWO_3$ is also shown by solid and dashed lines for comparison. Open circles show the highest intensity in experimental band mapping. **(c)** Three-dimensional view of the calculated FSs of $NaWO_3$. **(d)** Projected FS in two-dimensional k_xk_y (ΓXMX) plane. **(e)** Fermi surfaces of $Na_{0.8}WO_3$ showing electron-like pocket at Γ(X) point. The calculated Fermi surface(s) (on ΓXMX and XMRM planes) are shown by dotted lines.

at E_F vanishes. Hence Anderson localization is responsible for the insulating properties observed for low Na-doped Na_xWO_3.

We have measured near-E_F ARPES spectra of metallic Na_xWO_3 for x ranging from 0.58 to 0.8 [14]. A typical ARPES spectrum for $x = 0.8$ at 14 K along Γ(X)-M(R) direction is shown in figure 7a. It has been found that all the features are similar for all metallic samples. A peak around $\sim$1.0 eV at Γ(X) disperses upward to form an electron-like pocket for all compositions of x. Figure 7b shows the experimental band structure near-E_F for Na_xWO_3, $x = 0.8$ along with superposition of theoretical band calculation. Electron-like band is clearly visible around the Γ(X) point. No signature of impurity band (level) near E_F is seen in any of the experimental band structure of metallic samples and rules out the development of a Na-induced impurity band (level) [8], which was one of the models to explain the observed MIT in Na_xWO_3. To understand the evolution of Fermi surface (FS) with Na doping, it is necessary to calculate FS for $NaWO_3$, where $x = 1$ and use rigid band model to derive FS for appropriate Na concentration. Figure 7c shows the three-dimensional FS of Na_xWO_3 ($x = 1$) in first Brillouin zone obtained using the FP-LAPW calculation and the projected Fermi surface in the k_xk_y plane is shown in figure 7d. It is observed that the total FS consists of one spherical electron-like FS centred at the Γ point, which is covered with another square-like FS. A cylindrical Fermi surface is also present as shown in figure 7d. Experimentally, the FS, which is the ARPES-intensity plot at E_F for Na_xWO_3 ($x = 0.8$) as a function of the k_x and k_y wave vectors is shown in figure 7e. The intensity is obtained by integrating the spectral weight within 20 meV with respect to E_F. FS topology for all metallic samples is similar in nature. Theoretically calculated FS on ΓXMX and XMRM plane of BZ for $x = 0.8$ is superimposed on experimental FS for comparison. It has been found that there is an excellent match between theoretical and experimental FS(s). We observed one spherical electron-like FS centred at the Γ(X) point, which is covered with another square-like FS as predicted by calculation (see figure 7d).

4. Conclusion

Photoemission spectroscopy on Na_xWO_3 for insulating ($x = 0.025$) and metallic ($x = 0.58$–0.8) compositions has been performed. Experimental band structures have been compared with the FP-LAPW band calculations of $NaWO_3$. We found that the near-E_F states are localized in insulating sample due to random distribution of Na in WO_3 lattice and Anderson localization is responsible for the observed MIT in Na_xWO_3. Our spectromicroscopic study on both insulating and metallic samples does approve percolation model within experimental limit as one of the explanations for MIT. We could not find any signature of impurity band (level) near E_F in the metallic regime. Hence our result discards the Na-induced impurity band model as the origin of MIT. We observed electron-like Fermi surface(s) for metallic samples at the Γ(X) point which shows good agreement with band calculation.

References

[1] C G Granqvist, *Handbook of inorganic electrochromic materials* (Elsevier, Amsterdam, 1995)

[2] P M S Monk, R J Mortimer and D R Rosseinsky, *Electrochromism: Fundamentals and applications* (VCH, Weinheim, 1995)
[3] S Raj, T Sato, S Souma, T Takahashi, D D Sarma and P Mahadevan, *Mod. Phys. Lett. B* **23**, 2819 (2009)
[4] A S Ribnick, B Post and E Banks, *Adv. Chem. Ser.* **39**, 246 (1963)
[5] H R Shanks, P H Slides and G C Danielson, *Adv. Chem. Ser.* **39**, 237 (1963)
[6] A R Mackintosh, *J. Chem. Phys.* **38**, 1991 (1963)
[7] P W Anderson, *Phys. Rev.* **109**, 1492 (1958)
[8] D P Tunstall and W Ramage, *J. Phys. C: Solid State Phys.* **13**, 725 (1980)
[9] S Oishi, N Endo and K Kitajima, *Nippon Kagaku Kaishi* No. **11** p. 891 (The Chemical Society of Japan, Japan, 1995)
[10] H R Shanks, *J. Crystal Growth* **13**/**14**, 433 (1972)
[11] S Paul, A Ghosh, P Dudin, A Barinov, A Chakraborty, S Ray, D D Sarma, S Oishi and S Raj, *Solid State Commun.* **166**, 66 (2013)
[12] P Dudin, P Lacovig, C Fava, E Nicolini, A Bianco, G Cautero and A Barinov, *J. Synchrotron Radiat.* **17**, 445 (2010)
[13] A Einstein, *Ann. Der Physik* **325**, 199 (1906)
[14] S Raj, D Hashimoto, H Matsui, S Souma, T Sato, T Takahashi, S Ray, A Chakraborty, D D Sarma, P Mahadevan, W H McCarroll and M Greenblatt, *Phys. Rev. B* **72**, 125125 (2005)
[15] S Raj, D Hashimoto, H Matsui, S Souma, T Sato, T Takahashi, D D Sarma, P Mahadevan and S Oishi, *Phys. Rev. Lett.* **96**, 147603 (2006)
[16] S Raj, H Matsui, S Souma, T Sato, T Takahashi, A Chakraborty, D D Sarma, P Mahadevan, S Oishi, W H McCarroll and M Greenblatt, *Phys. Rev. B* **75**, 155116 (2007)
[17] S Raj, A Chakraborty, D Choudhury, T Sato, T Takahashi, P Mahadevan, J Fujii, I Vobornik and D D Sarma, *Phys. Rev. B* **79**, 035119 (2009)
[18] S Paul, A Ghosh, A Chakraborty, L Petaccia, D Topwal, D D Sarma, S Oishi and S Raj, *Solid State Commun.* **152**, 493 (2012)
[19] N F Mott, *Phil. Mag.* **35**, 111 (1977)
[20] D J Singh and L Nordström, *Plane waves, pseudopotentials and the LAPW method* (Springer, New York, 2006)
[21] ELK code: http://elk.sourceforge.net